Inhibition of Tumor Growth and Elimination of Multiple Metastases in Human Prostate and Breast Xenografts by Systemic Inoculation of a Host Defense–Like Lytic Peptide

Niv Papo,[1] Dalia Seger,[2] Arik Makovitzki,[1] Vyacheslav Kalchenko,[3] Zelig Eshhar,[4] Hadassa Degani,[2] and Yechiel Shai[1]

Departments of [1]Biological Chemistry, [2]Biological Regulation, [3]Veterinary Resources, and [4]Immunology, The Weizmann Institute of Science, Rehovot, Israel

Abstract

We report on a short host defense–like peptide that targets and arrests the growth of aggressive and hormone-resistant primary human prostate and breast tumors and prevents their experimental and spontaneous metastases, respectively, when systemically inoculated to immuodeficient mice. These effects are correlated with increased necrosis of the tumor cells and a significant decrease in the overall tumor microvessel density, as well as newly formed capillary tubes and prostate-specific antigen secretion (in prostate tumors). Growth inhibition of orthotopic tumors derived from stably transfected highly fluorescent human breast cancer cells and prevention of their naturally occurring metastases were visualized in real time by using noninvasive whole-body optical imaging. The exclusive selectivity of the peptide towards cancer derives from its specific binding to surface phosphatidylserine and the killing of the cancer cells via cytoplasmic membrane depolarization. These data indicate that membrane disruption can provide a therapeutic means of inhibiting tumor growth and preventing metastases of various cancers. (Cancer Res 2006; 66(10): 5371-8)

Introduction

Our immune system is geared to recognize and destroy cancer cells mainly through receptor-mediated mechanisms (1–3). Despite evidence that immune effectors can play a significant role in controlling tumor growth under natural conditions or in response to therapeutic manipulation, cancer cells usually evade immune surveillance (1). In that regard, host defense–derived cytolytic cationic polypeptides, which were initially discovered due to their role in clearance of bacteria (for reviews, see refs. 4–7), seem to overcome these limitations via a yet unknown non-receptor-mediated mechanism (8–13).

These peptides bind strongly to negatively charged membranes (4, 5, 14–18) and lyse them (19, 20). The outer membrane of cancer cells contains small amounts of negatively charged phosphatidylserine (3-9%; refs. 21, 22), being slightly more negative than that of nonmalignant eukaryotic cells. Whether this small difference in the membrane composition suffices to explain the ability of some cationic peptides to preferentially kill cancer cells is still not clear (23–25). Interestingly, however, surface-exposed phosphatidylserine also serves as a marker for the clearance of cancer cells from the bloodstream by innate immunity effectors such as monocytes, although through a completely different (receptor-mediated) mechanism (26). It has been suggested that the actual killing of cancer cells by cationic peptides is the result of one of the two processes: (*i*) induction of necrosis resulting from the disruption of the cytoplasmic membrane (20, 25) or (*ii*) induction of apoptosis triggered by the binding of the peptides to the mitochondrial membrane (9, 27).

To date, only a few successful attempts have been made *in vivo* with peptides capable of disrupting membranes and subsequently causing cancer cell death. These studies include (*i*) systemic treatments of solid tumors with lytic peptides, but only when they were conjugated to homing (targeting) domains or when used as propeptides (12, 27), mainly because the lytic entity is inactivated in serum and lacks tumor specificity; (*ii*) treatment of ovarian cancer with magainin and its D-amino acid enantiomer, but only when injected i.p. at high doses (28); and (*iii*) an intratumor administration of a 69-amino-acid pore-forming peptide against human breast cancer xenografts (11). Importantly, all of these treatments influenced only slightly, if at all, disseminated metastases (27) because of either limited intrinsic local activity or their inability to reach sizeable metastases in the intact animals. Furthermore, to date, the selectivity of cytotoxic peptides to cancer and their toxicity to other healthy organs have not been reported. We have recently shown that an intratumor injection of a short 15-mer D,L-amino acid peptide (D-K_6L_9; LK*L*LK*K*LL*K*KLL*K*LL-NH_2, italic letters are D-amino acid) inhibited the growth of primary human prostate carcinomas without affecting the nonmalignant neighboring cells (13).

Strikingly, we show here that D-K_6L_9 specifically targets and inhibits the growth of primary and metastatic tumors when administered systemically. Studies of its unique mode of action support the extracellular membrane phosphatidylserine as the target for this peptide, which acts via a membrane-depolarizing lytic mechanism.

Materials and Methods

Cell Culture

The CL1 human prostate carcinoma cell line used is an AI subclone of LNCaP, which was generated by culturing adenocarcinoma LNCaP cells in charcoal-stripped serum as previously described (29). The 22RV1 human prostate carcinoma cells are AI subclones of the adenocarcinoma prostatic adenocarcinoma CWR22 xenograft (30). The CL1 and 22RV1 [American Type Culture Collection (ATCC), Manassas, VA] were grown in RPMI 1640 supplemented with 10% FCS (Biological Industries, Beit Haemek, Israel). Extremely high-fluorescence estrogen receptor α–negative MDA-MB-231 human breast cancer cells (RFP-MDA-MB-231) were obtained by stable

Note: Y. Shai has the Harold S. and Harriet B. Brady Professorial Chair in Cancer Research. H. Degani is the incumbent of the Fred and Andrea Fallek Professorial Chair in Breast Cancer Research.

Requests for reprints: Yechiel Shai, Department of Biological Chemistry, The Weizmann Institute of Science, Rehovot, 76100 Israel. Phone: 972-8-934-2711; Fax: 972-8-934-4112; E-mail: Yechiel.Shai@weizmann.ac.il.

©2006 American Association for Cancer Research.

doi:10.1158/0008-5472.CAN-05-4569

Downloaded from http://aacrjournals.org/cancerres/article-pdf/66/10/5371/2548766/5371.pdf by guest on 16 January 2025

transfection with *pDsRed2-N1* (Clontech, Palo Alto, CA).[5] These cells express red fluorescence protein constantly with no reduction in intensity over time both *in vitro* and *in vivo*. The cells were maintained in RPMI 1640 supplemented with 1 mmol/L sodium pyruvate, 10% FCS, and 0.8 mg/mL G418. NIH 3T3 mouse fibroblast cell lines (ATCC) were grown in DMEM supplemented with 10% fetal bovine serum. OL human foreskin fibroblasts (ATCC; a generous gift from Prof. Menachem Rubinstein, Department of Molecular Genetics, Weizmann Institute of Science, Rehovot, Israel) were maintained in 10% FCS and DMEM. RWPE-1 human epithelial prostate cells (ATCC; a generous gift from Prof. Yosef Yarden, Department of Biological Regulation, Weizmann Institute of Science, Rehovot, Israel) were maintained in keratinocyte serum-free medium (Life Technologies, Inc., San Diego, CA) supplemented with 5 ng/mL human recombinant epidermal growth factor (EGF) and 0.05 mg/mL bovine pituitary extract (31). Immortalized 1306N and 2783N human breast cells taken from healthy breast tissues of patients with breast cancer (a generous gift from Prof. Lea Eisenbach, Department of Immunology, Weizmann Institute of Science, Rehovot, Israel) were maintained in DMEM/F-12 medium supplemented with 5 ng/mL EGF, 5 μg/mL hydrocortisone, 0.5 ng/mL T3 hormone, 0.5 ng/mL estradiol, 1% glutamine, 1% FCS, and antibiotics.

Studies with Prostate Carcinoma Xenografts

Solid tumor model. All animal experiments were done according to regulations approved by the Institutional Animal Care and Use Committee.

S.c. implantation of human prostate carcinoma in mice was done as previously described (32). Briefly, 0.1 mL AI 22RV1 human prostate carcinoma cells (5×10^6 cells) in Matrigel (Biological Industries) was inoculated s.c. into the dorsal side of 5- to 6-week-old nude male mice weighing 20 to 25 g (Harlen Co., Rehovot, Israel). Two weeks after cell implantation (tumor diameter, ~5 mm), D-K_6L_9 (at 9 mg/kg, 0.14 mmol/L) or vehicle (PBS, pH 7.4) was injected systemically (dosing volume of 45 mL/kg) thrice a week (every second day) for a total of nine doses per mice (n = 10 mice per group). Mice were weighed and the tumor size was measured by a caliper and recorded twice a week for a period of 40 days. At the end of the treatment, the mice were sacrificed and the tumors were removed, photographed, and weighed.

Serum prostate-specific antigen levels. Blood samples, taken 4 weeks after the first treatment with the 22RV1-inoculated mice, were collected into heparin-containing tubes, centrifuged, and the supernatants were stored at −20°C. The CanAg prostate-specific antigen EIA kit (CanAg Diagnostics, Gothenburg, Sweden) was used to determine the total prostate-specific antigen in the mice plasma (32). Tumor size and prostate-specific antigen levels, represented as mean ± SE, were analyzed by Student's t test. $P < 0.05$ was considered as statistically significant.

Histologic and immunofluorescent staining. Excised tumors were fixed in 4% buffered formaldehyde. Paraffin-embedded 5-μm sections were stained with H&E. The percentage of necrotic area of the total section area was calculated using the Image-Pro plus 4.1 software.

Immunofluorescent staining was done as previously described (33). Briefly, paraffin-embedded 5-μm tumor sections were overlaid with rabbit anti–von Willebrand antibody (Chemicon, Temecula, CA) or rat anti-CD34 antibody (Accurate Chemicals, Torrance, CA) against blood vessels. Sections were incubated with bridging biotinylated goat anti-rabbit and rabbit anti-rat antibodies (Vector Laboratories, Burlingame, CA), respectively, and visualized with streptavidin-biotin conjugated with FITC (Jackson ImmunoResearch Laboratories, West Grove, PA). For quantitative analysis, capillaries, identified by positive staining for CD34 and von Willebrand, were counted and their density was expressed as the percentage of capillaries of the total section area using Image-Pro plus 4.1 software. To quantify the vessels, 10 nonnecrotic areas at 100 μm^2 per field at ×200 were captured for each tumor using an Olympus BX-40 microscope (Olympus, Tokyo, Japan). Macrophage cells, identified by their specific morphology and color, were counted and their density in the whole section area was calculated using Matlab program and Image-Pro plus 4.1 software. For that purpose, 20 nonnecrotic areas (at 100 μm^2 per field at ×200) from tumors of treated and untreated mice were captured for each tumor using an Olympus BX-40 microscope.

Experimental metastasis model. Five- to six-week-old nude male mice weighing 20 to 25 g (Harlen) were injected i.v. with 1×10^6 metastatic 22RV1 prostate carcinoma cells (34). After 24 hours, the animals were randomly assigned into groups (n = 10 mice per group). D-K_6L_9 at 9 mg/kg or the control (PBS, pH 7.4) at 45 mL/kg was administered i.v. to the mice every day for 3 days in the first week and then once a week for the next 2 weeks, for a total of five treatments for a period of 21 days. Mice were weighed and recorded twice a week for a period of 60 days. On day 60, the mice were sacrificed and their lungs were removed, fixed in 4% buffered formaldehyde, and paraffin-embedded 5-μm sections were stained with H&E to measure the extent of lung metastases.

In vivo Optical Imaging in Breast Cancer Xenografts

Spontaneous metastasis model. RFP-MDA-MB-231 breast cancer cells were injected (5×10^6 cells in 0.1 mL PBS) into the left mammary fat pad of 8-week-old female SCID/NCr mice (National Cancer Institute, Bethesda, MD) as previously described (35). One week after cell implantation (~5 mm tumor diameter), D-K_6L_9 (at 5 mg/kg, 0.14 mmol/L) or vehicle (PBS, pH 7.4) was injected systemically (dosing volume of 22 mL/kg) thrice a week (every second day) for a total of nine doses for 10 mice, respectively. Mice were weighed and tumor volume was measured by a caliper (expressed in weight units (mg); ref. 20) twice a week for a period of 45 days.

Primary tumor and metastases fluorescence were detected noninvasively using an *in vivo* optical imaging system (IVIS-100, Xenogen Corp., Alameda, CA) with excitation and emission filters at 500 to 550 and 575 to 650 nm, respectively. Tumor fluorescence intensity and areas were recorded once a week for a period of 45 days after cell implantation. At the end of the experiment, the mice were sacrificed and the lungs and lymph nodes were removed and monitored for fluorescent metastases. Lungs and lymph node sections, stained with H&E, were used for calculating metastatic areas.

To noninvasively visualize micrometastases in living animals, we used a Zoom Stereo Microscope SZX-RFL-2 (Olympus) equipped with a fluorescence illuminator and a CCD camera Pixelfly QE (PCO, Kelheim, Germany). The excitation and emission filter set was 460 to 560 and 590 nm (long pass), respectively. ImageJ 1.330 software by Wayne Rasband was used for image analysis.

Binding and colocalization *in vitro*. All cells investigated were seeded at 1×10^4 per well on six-well plates and grown for 24 hours in complete medium. Cells were then incubated with 1 μmol/L NBD-labeled D-K_6L_9 for 30 minutes at 37°C, washed, dissociated from the wells, and placed in flow cytometry tubes. NBD fluorescence was measured (excitation 488 nm, emission 525 nm) using a FACScan (Becton Dickinson, Franklin Lakes, NJ). Mean fluorescence intensity per cell corresponds to the amount of cell-associated peptide. Data were reported as mean ± SD for at least triplicates. An inactive 12-mer synthetic peptide served as a negative control.

To follow peptide-membrane phosphatidylserine colocalization, CL1 and 22RV1 prostate carcinoma and MB-231 breast cancer cells were seeded at 1×10^4 per chamber in a chambered cover glass system (Lab-Tek, Campbell, CA) and grown for 24 hours in complete medium. Thereafter, cells were washed and preincubated with Annexin V-FITC (Sigma, St. Louis, MO), which detects cell-surface phosphatidylserine. Subsequently, the cells were incubated with the Rho-labeled D-K_6L_9 for 30 minutes at 37°C, washed, and observed on an Olympus IX70 FV500 confocal laser scanning microscope. FITC and Rho fluorescence on the cell surface were analyzed quantitatively. The confocal images were obtained at 12-bit resolution.

Analysis of D-K_6L_9-Treated Damaged Cells

Fluorescenct confocal microscopy. Cultures of cells at 80% confluence were treated with 10 μmol/L D-K_6L_9 for 15 minutes at 37°C and then stained with the fluorescent dyes Annexin V and propidium iodide for apoptosis/necrosis detection (Molecular Probes, Eugene, OR). The apoptotic doxorubicin served as a control.

Flow cytometry. Cells were treated with 10 μmol/L D-K_6L_9, harvested with trypsin-EDTA, washed, resuspended in medium, and then treated with the fluorescent dyes diS-C_3-5 and propidium iodide (Molecular Probes) to follow simultaneously membrane depolarization and cell viability, respectively.

[5] Dadiani M. et al., submitted for publication.

Downloaded from http://aacrjournals.org/cancerres/article-pdf/66/10/5371/2548766/5371.pdf by guest on 16 January 2025

Results

We used in this study, in addition to D-K_6L_9, two peptides as controls: (*i*) the parental L-amino acid version of D-K_6L_9, which is highly potent toward cancer and noncancer cells (13), and (*ii*) a 12-mer peptide D-K_5L_7 (KLLLKLKLKLLK-NH_2, underlined letters are D-amino acid), which permeates negatively charged membranes and kills bacteria similarly to D-K_6L_9, but not cancer cells.

Inhibition of solid prostate cancer growth and prostate-specific antigen secretion by D-K_6L_9. Two weeks after implantation, D-K_6L_9 was systemically injected (every second day) at a dose of 9 mg/kg (LC_{50} of 6 μmol/L against cultured 22RV1 prostate carcinoma cells). The major reduction in tumor size (Fig. 1*A* and *B*) was observed from day 20 until day 38, during which the tumor size decreased by >3-fold (Fig. 1*C*). The reduction in tumor size was accompanied by a marked lowering of the 22RV1-secreted (30) prostate-specific antigen serum levels (Fig. 1*D*) and an increase in the body weight (from 35 to 45 g) of treated animals compared with the control group. In contrast, the parental L-K_6L_9 was inactive in this model (data not shown), probably because it is fully inactivated by proteolytic enzymes that exist in the tumor extracellular matrix or blood, whereas D-K_6L_9 preserves ~50% activity (13). The second inactive control, the antimicrobial peptide D-K_5L_7, although preserving antimicrobial activity in serum, is not hydrophobic enough to lyse mammalian cells (data not shown).

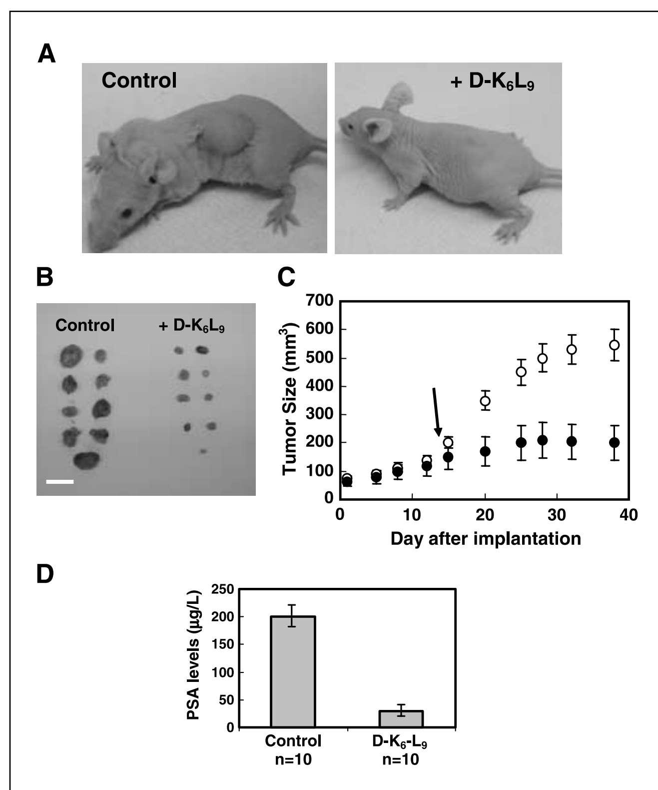

Figure 1. Reduction in the size of s.c. implanted 22RV1 prostate tumors during i.v. treatment with D-K_6L_9 (nine doses of 9 mg/kg each). *A,* dorsal side of nude male mice s.c. injected with 22RV1 tumor cells and i.v. treated with D-K_6L_9 (*right*) or vehicle control (*left*). *B,* exposed tumors (at day 40 after cell implantation) of mice treated with D-K_6L_9 or vehicle control. Bar, 9 mm. *C,* tumor growth curve of postadministration of D-K_6L_9 (●) or vehicle control (○). n = 10 animals. P = 0.002, t test. *Bars,* SD. *Arrow,* first peptide injection. *D,* prostate-specific antigen (*PSA*) serum levels (at day 40 after cell implantation) in mice described in (*C*). P = 0.004, t test. *n,* number of animals. *Bars,* SE.

To examine the possible mechanisms underlying tumor growth arrest, we excised and stained with H&E tumors taken 6 weeks after cell implantation. Histologic analysis revealed that the tumors in the control-untreated mice (Fig. 2*A*) were enlarged and were populated entirely by the cancer cells. In contrast, the tumors in D-K_6L_9-treated mice were much less densely populated. Furthermore, quantification of necrotic areas in three sections of each tumor (calculated for three tumors) revealed that the necrotic area in the tumors from D-K_6L_9-injected mice was 10-fold larger than the necrotic area found in the tumors of untreated mice. At day 40 after cancer cell implantation, the amount of macrophages in the whole section area, represented as mean ± SE, was analyzed by Student's t test. $P < 0.05$ was considered as statistically significant. The analysis revealed a 3-fold more macrophages in the treated tumors compared with the untreated tumors. This is illustrated in the magnified slices in Fig. 2*A*. We therefore cannot rule out an additional mechanism for tumor elimination by the peptide, which involves the recruitment and induction of host defense effector cells at the tumor area. Recent studies have shown that D-K_6L_9 and similar cationic lytic peptides do not stimulate macrophages to release proinflammatory cytokines, such as tumor necrosis factor α and interleukin-6 (36). Therefore, we believe that the function of the macrophages is mainly to clean up the cellular debris. Further quantitative analysis of the difference in capillary density was done on three tumors and at least three sections per tumor (Fig. 2*B*). Overall microvessel (old and new blood vessels) and newly formed capillary tube densities of tumors resulting from the D-K_6L_9-treated mice, obtained from both von Willebrand and CD34 staining, respectively, were remarkably reduced (8 and 13 times, respectively) as compared with those of tumors from untreated mice ($P < 0.005$).

D-K_6L_9 prevents prostate 22RV1 tumor experimental lung metastases. Systemic inoculation of D-K_6L_9 significantly inhibited lung metastases compared with the untreated or D-K_5L_7-treated controls (Fig. 2*C*). Furthermore, the treated mice also had a marked increase in their body weight compared with the vehicle-treated control group (Fig. 2*D*) and did not show signs of toxicity throughout the assay period.

D-K_6L_9 inhibits the growth of breast carcinoma and prevents spontaneous metastases spread. D-K_6L_9 was injected systemically (every second day) at a dose of 5 mg/kg (LC_{50} of 3 μmol/L against cultured MB-231 cells) starting 1 week after tumor cell implantation. Real-time, fluorescence whole-body optical imaging revealed a progressive increase in the primary tumor and multiple metastatic growth in all untreated animals. Specifically, fluorescent primary tumors were visible through the skin as early as 7 days after implantation. The noninvasive quantitative measurements of the externally visible fluorescent area (37) and total fluorescent intensity enabled us to construct *in vivo* tumor growth curves (Fig. 3*B*), which showed a remarkably linear tumor growth rate in the untreated animals. In contrast, a marked lowering of the tumor fluorescence intensity (Fig. 3*C*) and area (Fig. 3*B* and *C*) was observed for the treated animals. Note that the major reduction in tumor size, as recorded from caliper measurements, was observed from day 27 until day 45, reaching a 3.5-fold decrease in the mean size of the tumors (Fig. 3*A*). Interestingly, however, the significant reduction in the amount of the fluorescent tumor cells was observed already on day 15 and reached a 5-fold decrease in the mean fluorescence area of the tumors at day 45 (Fig. 3*B*), reflecting the higher accuracy of the IVIS technology.

Downloaded from http://aacrjournals.org/cancerres/article-pdf/66/10/5371/2548766/5371.pdf by guest on 16 January 2025

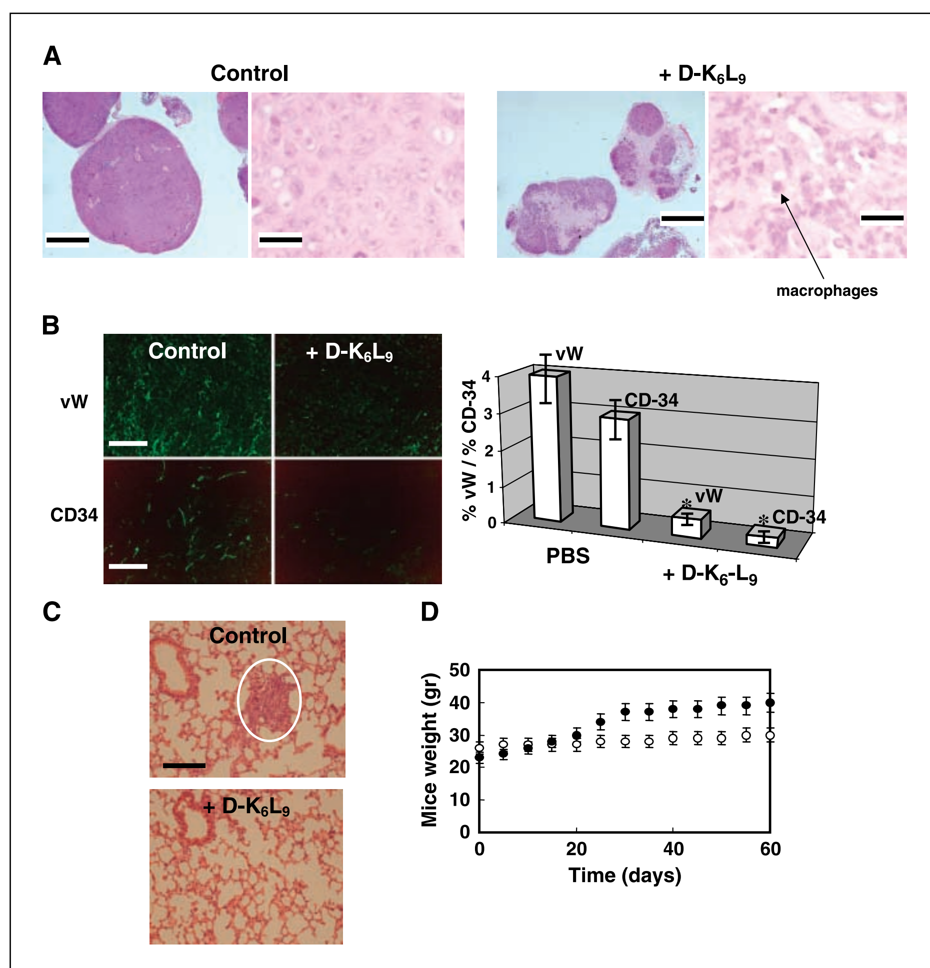

Figure 2. Histologic and immunohistochemical analysis of 22RV1 solid tumor (primary tumor model) and lung (metastatic model) sections after treatment with 9 mg/kg of D-K_6L_9. *A,* histologic analysis (H&E staining) of primary tumors (paraffin-embedded 5-μm sections) after treatment with D-K_6L_9 (*right*) or vehicle control (*left*). Bar, 3 mm for low magnification and 250 μm for high magnification. *Arrow,* macrophages. *B,* decreased vascularization of solid tumors formed in the D-K_6L_9-treated animals as compared with tumors from untreated animals. Sections were stained with Von Willebrand (*vW*; *top*) and CD34 (*bottom*) antibodies (as described in Materials and Methods) to visualize total capillary density and newly formed microvessel tubes in the tumors, respectively. Bar, 0.1 mm. *Right,* capillary density was calculated as the percentage of von Willebrand– or CD34-positive areas of the total section area. Analysis was done on three tumors and at least three sections per tumor. *, $P = 0.001$, significant difference between untreated and treated animals for both von Willebrand and CD34 staining. *C,* H&E staining of lung sections (taken from the D-K_6L_9-treated CD1 nude mice bearing 22RV1 tumors) showing no metastases. *Circle,* lung metastases that exist in the untreated animals. Bar, 1 mm. Lung metastasis resulted from systemic inoculation of 22RV1 prostate carcinoma cells (1×10^6). The peptide treatment included five doses of 5 mg/kg (as described in Materials and Methods). *D,* increase in body weight of mice i.v. injected with 22RV1 prostate carcinoma cells and then treated with D-K_6L_9 (●) as compared with untreated mice (○). $n = 10$ animals. $P = 0.003$, *t* test. *Bars,* SD.

Downloaded from http://aacrjournals.org/cancerres/article-pdf/66/10/5371/2548766/5371.pdf by guest on 16 January 2025

The development of both nearby (lymph node) and distant (lung) tumor metastases were identified in all animals by day 45. Whole-body stereo-microscope fluorescence imaging (at day 45) of metastases in the pelvic areas in mice untreated (Fig. 3*D, top*) and treated with d-K6L9 (Fig. 3*D, bottom*) showed their elimination in the treated mice. The IVIS system did not allow efficient detection of the lung fluorescence through the chest, and therefore the exposed lungs are shown (Fig. 4*A*), which show a strong fluorescence in the untreated mice. The lungs of the treated mice show only the background autofluorescence similarly to lungs without metastases. Histologic analysis of dissected lungs and lymph nodes (Fig. 4*B*) confirmed that these organs were markedly more populated by the cancer cells in the control untreated mice compared with the treated mice. Metastasis quantification was done in areas from three sections of each organ ($P = 0.001$).

As mentioned above, to assess toxicity in mice without tumors, we systemically injected D-K_6L_9 to both CD1 nude and SCID mice at a dose of 5, 7, and 10 mg/kg thrice a week for 3 weeks. No apparent toxicities were found in 4 months.

D-K_6L_9 selectively interacts with cancer cells. The activity (LC_{50}) of D-K_6L_9 on the cancer cells [22RV1 prostate carcinoma (6 μmol/L), CL1 prostate carcinoma (3 μmol/L), and MB-231 breast cancer cells (3 μmol/L)] is higher than on the noncancer cells tested, which included NIH 3T3 (100 μmol/L), OL foreskin fibroblasts (35 μmol/L), human epithelial RWPE-1 prostate cells (40 μmol/L), and immortalized 1306N (20 μmol/L) or 2783N (20 μmol/L) human breast cells. The control peptide D-K_5L_7 was practically inactive on both cancer cells [22RV1 prostate carcinoma (>50 μmol/L) and CL1 prostate carcinoma (100 μmol/L)] and noncancer cells tested [NIH 3T3 (>100 μmol/L), OL foreskin fibroblasts (50 μmol/L), and human epithelial RWPE-1 prostate cells (>50 μmol/L)]. In contrast, the parental peptide L-K_6L_9 was highly active on both cancer [22RV1 prostate carcinoma (4 μmol/L), CL1 prostate carcinoma (4 μmol/L), and MB-231 breast cancer cells (4 μmol/L)] and noncancer cells [NIH 3T3 (7 μmol/L) and OL foreskin fibroblasts (5 μmol/L)]. To better understand this selectivity, we incubated all the cells for 30 minutes with 1 μmol/L (a sublethal concentration) of NBD-labeled peptides (D-K_6L_9 and its inactive variant, 12-mer; ref. 13) and measured the cellular association using flow cytometry. As shown in Fig. 5*A* (*left*), the NBD-D-K_6L_9 treatment shifted the NBD-fluorescence profile of the cancer cells (22RV1 are shown as an example) to the right (95 ± 5% peptide bound cells), but only slightly (only 10 ± 1% peptide bound cells) in the case of noncancer cells (3T3 fibroblasts are shown as an example). In contrast, the inactive variant did not bind both types of cells (Fig. 5*A, right*). Similar results were obtained when we compared other cancer cells (CL1 prostate carcinoma and MB-231 breast cancer cells) with noncancer cells (OL fibroblasts, epithelial RWPE-1 prostate cells, and 1306N or 2783N human breast cells).

D-K_6L_9 targets and colocalizes with membrane phosphatidylserine. Confocal microscopy images of CL1 prostate carcinoma cells preincubated with Annexin V-FITC (for surface

phosphatidylserine detection) and then treated with rhodamine (Rho)-labeled (38) D-K_6L_9 showed colocalization of the red rhodamine and the green Annexin V-FITC fluorescence at 37°C (yielding yellow fluorescence; Fig. 5*B*). D-K_6L_9 was exclusively associated with the phosphatidylserine on the cell membrane (Fig. 5*C*) because there was no intracellular signal, indicating no detectable peptide internalization either into the cytosol or into the nucleus of the cell. Similar results were obtained for 22RV1 prostate carcinoma and MB-231 breast cancer cells (data not shown). Note that labeling the peptide with either NBD or Rho did not affect its antitumor activity.

D-K_6L_9 triggers necrosis via membrane depolarization. We treated CL1 (or 22RV1) prostate carcinoma cells (Fig. 6*A*) or 3T3 fibroblasts (Fig. 6*B*) with D-K_6L_9 or with the proapoptotic doxorubicin drug, followed by staining with FITC-Annexin V and propidium iodide. FITC-Annexin V binds exclusively to phosphatidylserine, which is exposed on the outer leaflet of the plasma membrane of cells in the initial stages of apoptosis, whereas propidium iodide preferentially stains the nucleus of necrotic cells with impaired membranes. Figure 6*A* (*right*) shows that treatment of prostate carcinoma cells with D-K_6L_9 induced necrosis (both Annexin V and propidium iodide positive). In contrast, doxorubicin induced only an apoptotic effect against the same cells (Annexin V positive, propidium iodide negative; data not shown). A similar apoptotic effect was observed with doxorubicin against the 3T3 fibroblasts (Annexin V positive, propidium iodide negative; Fig. 6*B, right*). Note that untreated prostate carcinoma cells (Fig. 6*A, left*) were richer in membrane-exposed phosphatidylserine as compared with untreated normal fibroblast cells (Fig. 6*B, left*).

To examine whether the necrotic effect results from the disruption of the cytoplasmic membrane, we used diS-C3-5 staining, which only stains cells with polarized cytoplasmic membranes. As shown in Fig. 6*C*, treatment with D-K_6L_9 (*right*) caused a shift in the fluorescence profile to more red (dead cells) and less blue (depolarized membranes), showing that the cancer cell death as a result of D-K_6L_9 treatment was due to membrane depolarization. In contrast, the control 12-amino-acid analogue (13) was inactive in this experiment (Fig. 6*D, left*). These results were obtained for CL1 prostate carcinoma, 22RV1 prostate carcinoma, and MB-231 breast cancer cells (shown only for CL1). All together, these data suggest that D-K_6L_9 induces necrosis by damaging the cytoplasmic membrane of these cancer cells.

Discussion

We showed for the first time that a short membrane-active peptide carries two functions: it recognizes and lyses cancer cells of

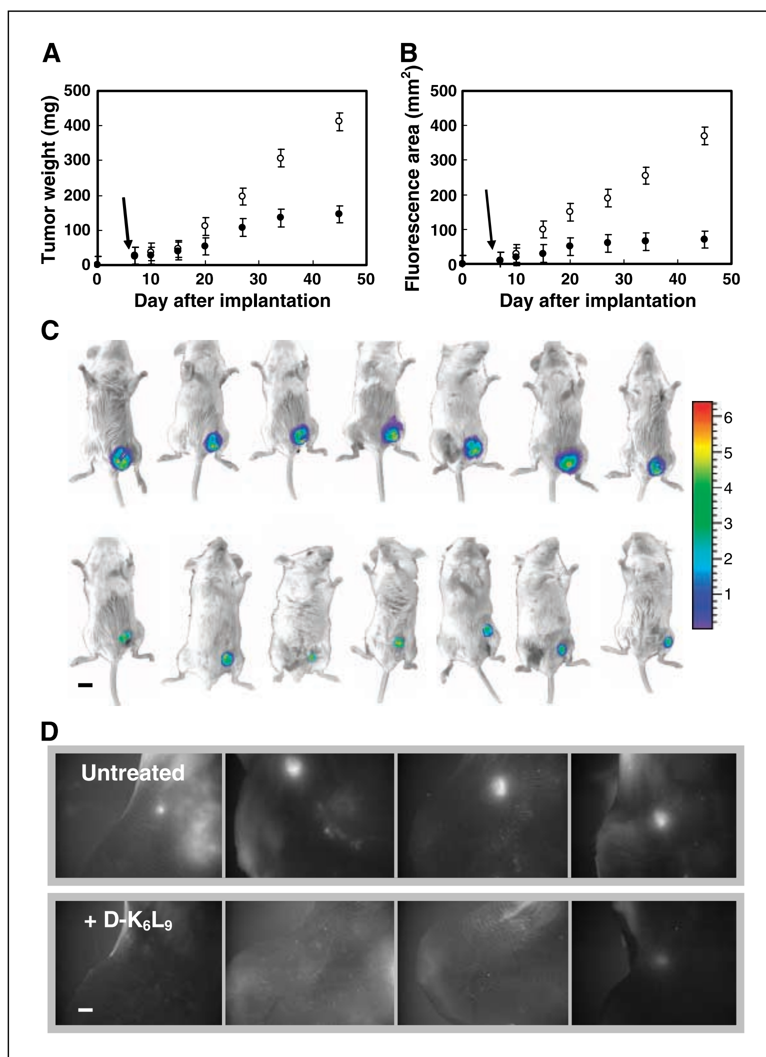

Figure 3. *In vivo* fluorescence imaging detecting the inhibition of orthotopic human breast RFP-MDA-MB-231 tumor growth in SCID/NCr female mice during i.v. treatment with 5 mg/kg of D-K_6L_9 (total of nine injections, thrice a week). *A,* tumor growth curve during treatment with D-K_6L_9 (●) or vehicle control (○). *B,* average fluorescence area (±SD) in the RFP-MB-231 tumor regions as a function of time after the start of treatment with D-K_6L_9. $n = 10$ animals. $P = 0.001$, *t* test. *Bars,* SD. *Arrow,* first injection of peptide (*A* and *B*). *C, in vivo* whole-body fluorescence imaging of mice bearing human breast RFP-MB-231 tumors in D-K_6L_9-treated (*bottom*) and untreated (*top*) mice. Bar, 2 cm. *D, in vivo* whole-body stereomicroscope fluorescence imaging of micrometastases in the lymph nodes in mice bearing human breast RFP-MB-231 tumor xenografts untreated (*top*) and treated with D-K_6L_9 (*bottom*). *C* and *D,* pictures at day 45 after implantation. Bar, 1 cm.

Downloaded from http://aacrjournals.org/cancerres/article-pdf/66/10/5371/2548766/5371.pdf by guest on 16 January 2025

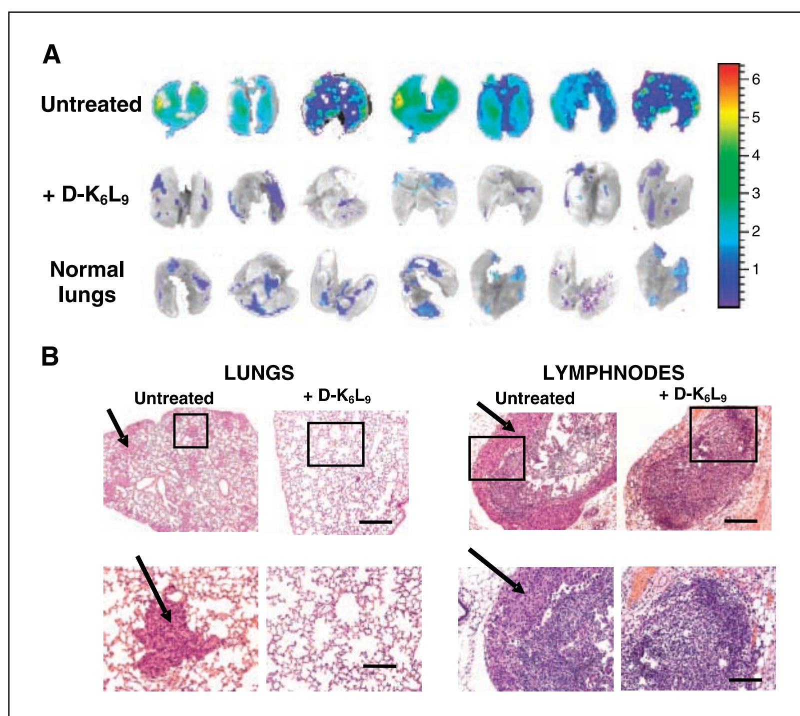

Figure 4. *A,* representative images of exposed lungs of SCID/NCr female mice bearing human breast RFP-MB-231 tumors untreated (*top*) and treated with D-K_6L_9 (*middle*). The tumors were obtained from injection of breast cancer cells into the mouse left mammary fat pad. Pictures taken 45 days after cell implantation. *Bottom,* lungs of normal (control) mice, for comparison. Blue color (low intensity value) seen in the lungs of treated mice is due to autofluorescence also shown in the control lungs. *B,* RFP-MB-231 metastases observed in lung and lymph node sections (H&E staining) obtained from the D-K_6L_9-treated mice as compared with lung and lymph node sections from untreated mice. *Bottom,* ×4 magnifications of the framed areas on the *top*. $P = 0.001$, *t* test. Bar, 100 μm (*top*); 25 μm (*bottom*). *Arrow,* metastasis.

primary tumors and spontaneous and experimental metastases. Furthermore, the data suggest that the tumor cells are lysed directly without the involvement of the adaptive immune system that is deficient in SCID mice.

Besides the drastic inhibition of tumor growth by D-K_6L_9 (Fig. 2*A*), the peptide also exhibited a 10-fold decrease in vascularization compared with the untreated mice (Fig. 2*B*). This may be the result of either the reduced cancer cell density, the induction

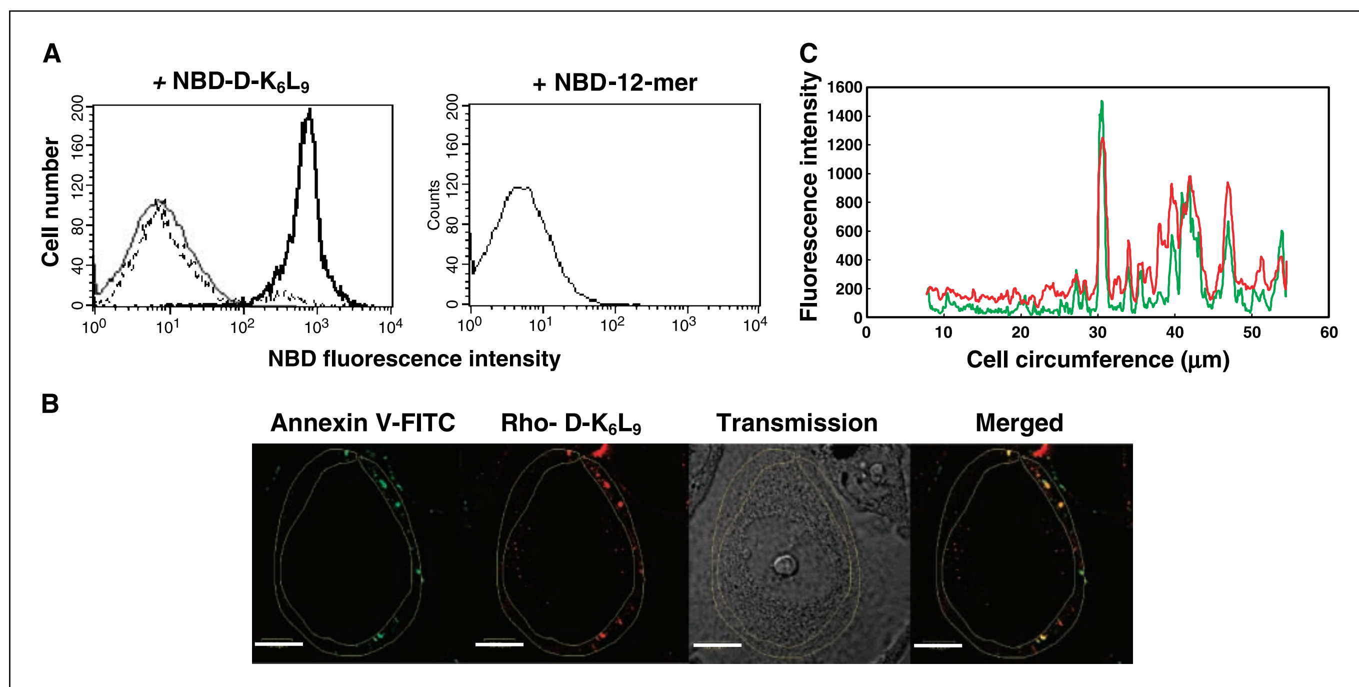

Figure 5. D-K_6L_9 selectively binds to cancer cells and colocalizes with their surface exposed phosphatidylserine. *A,* fluorescence-activated cell sorting analysis of 3T3 fibroblasts (*dotted line*), normal human epithelial RWPE-1 prostate carcinoma (*thin continuous line*), and 22RV1 prostate carcinoma cells (*thick continuous line*) treated with NBD-labeled D-K_6L_9 (*left*) or D-K_5L_7 (*right*). *Left,* D-K_6L_9 shifted the spectrum of the 22RV1 prostate carcinoma cells, but not that of the 3T3 fibroblasts or the normal epithelial prostate carcinoma, from left (unbound) to right (bound). *Right,* the inactive D-K_5L_7 did not shift the spectrum of any type of cells, indicating its inability to bind these cells. As expected, the control L-K_6L_9 shifted the spectrum of all the cells (data not shown). *B,* confocal laser scanning microscopy image of 1×10^4 CL1 prostate carcinoma cells, simultaneously treated (for 30 minutes) with Annexin V-FITC (detects exposed phosphatidylserine) and rhodamine-labeled D-K_6L_9. The D-K_6L_9 and the Annexin V-FITC were colocalized. Bar, 5 μm. *C,* quantitative analysis of the Annexin V-FITC and Rho-peptide fluorescence along the cell circumference as obtained from (*B*). We observe a quantitative colocalization of D-K_6L_9 and membrane outer leaflet–exposed phosphatidylserine.

Downloaded from http://aacrjournals.org/cancerres/article-pdf/66/10/5371/2548766/5371.pdf by guest on 16 January 2025

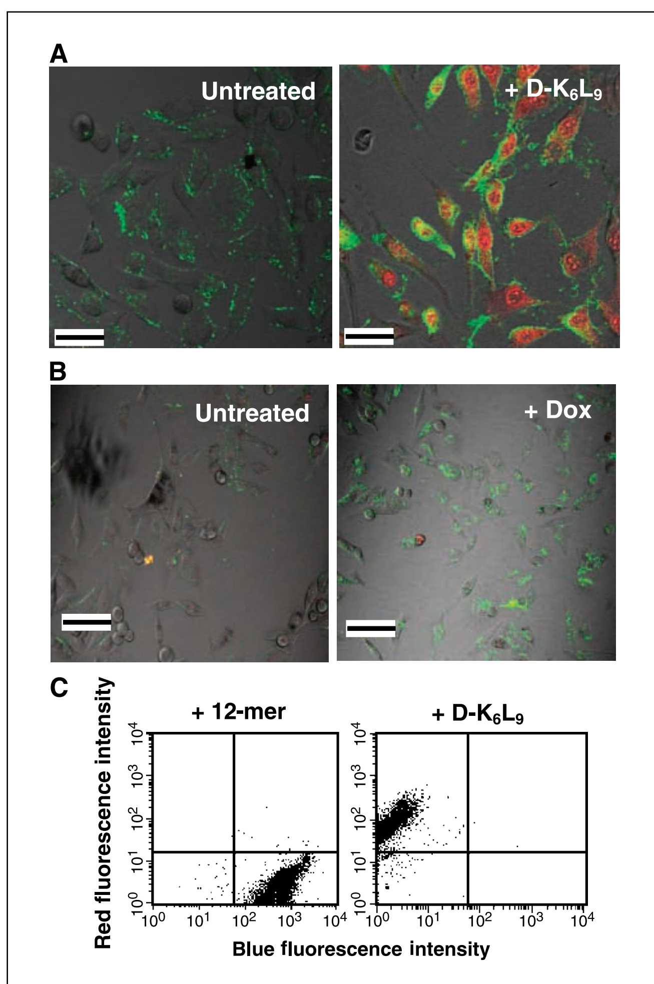

Figure 6. D-K_6L_9 depolarizes the membranes of prostate carcinoma cells as part of its cytotoxic effect. The D-K_6L_9 (10 μmol/L)–treated CL1 cells (*A, right*) were mostly necrotic (FITC-Annexin V and propidium iodide positive) whereas doxorubicin (*Dox*)-treated CL1 cells (not shown), which served as controls, were mostly apoptotic (FITC-Annexin V positive and propidium iodide negative). *B,* doxorubicin- treated (100 μmol/L) 3T3 fibroblast cells (*right*) were also mostly apoptotic. Note the significantly higher amounts of phosphatidylserine in the outer membrane of untreated CL1 prostate carcinoma cells as compared with the nonmalignant 3T3 fibroblasts (*A* and *B, left*). *C,* staining with diS-C_3-5 for membrane potential measurements. D-K_6L_9 shifted the spectrum of CL1 prostate carcinoma cells from low red (healthy) and high blue (full membrane potential) to high red (dead) and low blue (loss of membrane potential). The 12-mer, which had no effect on the cells, was used as an inactive control.

of angiogenic inhibiting factors (such as angiostatin ref. 39), or additional, yet unknown, vascular targeting and antiangiogenesis activity induced by the peptide. Inhibition of tumor growth by D-K_6L_9 was also accompanied by an increased number of cells containing necrotic debris in comparison with the significantly higher number of mitotic cells in the tumors of untreated mice (Fig. 1*A*). These results indicate that the observed reduction in tumor size is only an underestimation of the end point effect of D-K_6L_9 on the tumor cells. As for the long-term benefit of the treatment, in both prostate models (solid tumor and experimental metastasis), the animals were monitored for additional 3 months after the last treatment. Complete tumor eradication was observed in the solid tumor model with no increase in tumor size (figure not shown). In addition, in the prostate experimental metastasis model, 100% of the untreated mice died by day 75 after cell injection. In contrast, no mortality was observed for the treated animals even by day 165 after injection (end of the experiment; figure not shown). These data suggest that peptide treatment generates neither escape variants nor severe resistance. In addition, in a control experiment, the peptide was injected at a dose of 10 mg/kg for 7 consecutive days to 10 mice and no mortality was observed. A week later, blood samples were taken and we found that all the tests were in the range of normal values (i.e., levels of neutrophils, lymphocytes, monocytes, eosinophils, basophils, creatine phosphokinase, alkaline phosphatase, alanine aminotransferase, aspartate aminotransferase, and creatinine; data not shown).

The *in vivo* whole-body fluorescence imaging experiments revealed differences in peptide-induced reduction of primary human breast tumor weight and fluorescence (Fig. 3*A* and *B*). The accuracy of fluorescence detection is much greater because it reflects only tumor cells that are alive, and not necrotic or cystic regions,[5] which are not composed of cancer cells but do contribute to their total volume. Notably, both distant lung tumor metastases and adjacent lymph node metastases, which were clearly detected in the untreated intact animals, were completely absent in the treated animals (Fig. 3*D*). The lack of metastases in these organs, which was also confirmed on autopsy (Fig. 4), can be the result of either their prevention before the cancer cells settled and metastases were established or their elimination (or a combined effect).

The selectivity of D-K_6L_9 can be partially attributed to its ability to target surface-exposed phosphatidylserine in cancer cells (Fig. 5) that are enriched ~3-fold compared with the noncancer cells (21, 22, 40). This is in line with earlier reports that the peptide electrostatically binds phosphatidylserine-containing artificial membranes 2- to 3-fold better than phosphatidylserine-deficient membranes (41, 42). *In vivo* activity of D-K_6L_9 seems to be highly specific to cancer cells; therefore, should it bind to normal cells, it probably cannot reach a threshold lytic concentration (19) and therefore it will be washed out from the cells without causing any damage.

Both our *in vitro* and *in vivo* results suggest a two-step cytolytic effect which leads to necrosis (Fig. 6*A-C*). First, D-K_6L_9 binds to distinct sites on the cytoplasmic membrane of the cell and colocalizes with anionic phosphatidylserine (refs. 23, 24; Fig. 5*B* and *C*). Second, after a threshold concentration of the peptide is reached, a marked depolarization of the membrane occurs, leading to cell death (Fig. 6*D*). These steps are closely related to those observed with the cytolytic perforin (produced by killer lymphocytes), which damages its target cells by puncturing their membranes. However, in contrast to perforin, which facilitates access of natural killer or CTL-released proapoptotic serine protease to the cytoplasm of the target cell (43), our peptide lyses the target cell as part of an intrinsic property. However, we cannot rule out partial apoptosis, too.

There is no doubt that with the increasing resistance of cancer against conventional chemotherapy modalities, the D-K_6L_9 peptide described here has potentially desirable features characterizing a novel anticancer class of drugs. In particular, it has a broad spectrum of activity (25), acts rapidly (20), shows synergy with classic chemotherapy (13), prevents metastases, and does not destroy vital organs. Owing to its drastic membranolytic effect, it probably would be difficult for the cell to select chemotherapy-resistant variants, similarly to what has been found in many cases with bacteria treated with cationic innate immunity lytic peptides (4, 7).

Downloaded from http://aacrjournals.org/cancerres/article-pdf/66/10/5371/2548766/5371.pdf by guest on 16 January 2025

Acknowledgments

Received 12/27/2005; revised 2/15/2006; accepted 3/3/2006.

Grant support: Prostate cancer Foundation (Israel), the Prostate Cancer Research Foundation (UK), and in part by the Weizmann-Mario-Negri cooperation (H. Degani).

The costs of publication of this article were defrayed in part by the payment of page charges. This article must therefore be hereby marked *advertisement* in accordance with 18 U.S.C. Section 1734 solely to indicate this fact.

We thank T. Waks, Dr. R. Eilam, Dr. A. Harmelin, and V. Kiss for technical assistance and Profs. M. Rubinstein, Y. Yarden, and L. Eisenbach for providing us with some of the human cell lines used in this study.

References

1. Dunn GP, Bruce AT, Ikeda H, Old LJ, Schreiber RD. Cancer immunoediting: from immunosurveillance to tumor escape. Nat Immunol 2002;3:991–8.
2. Mocellin S, Rossi CR, Nitti D. Cancer vaccine development: on the way to break immune tolerance to malignant cells. Exp Cell Res 2004;299:267–78.
3. Blattman JN, Greenberg PD. Cancer immunotherapy: a treatment for the masses. Science 2004;305:200–5.
4. Boman HG. Peptide antibiotics and their role in innate immunity. Annu Rev Immunol 1995;13:61–92.
5. Hancock RE. Peptide antibiotics. Lancet 1997;349: 418–22.
6. Ganz T, Lehrer RI. Antimicrobial peptides of vertebrates. Curr Opin Immunol 1998;10:41–4.
7. Zasloff M. Antimicrobial peptides of multicellular organisms. Nature 2002;415:389–95.
8. Ohsaki Y, Gazdar AF, Chen HC, Johnson BE. Antitumor activity of magainin analogues against human lung cancer cell lines. Cancer Res 1992;52:3534–8.
9. Chen Y, Xu X, Hong S, et al. RGD-Tachyplesin inhibits tumor growth. Cancer Res 2001;61:2434–8.
10. Street SE, Cretney E, Smyth MJ. Perforin and interferon-γ activities independently control tumor initiation, growth, and metastasis. Blood 2001;97:192–7.
11. Ellerby HM, Lee S, Ellerby LM, et al. An artificially designed pore-forming protein with anti-tumor effects. J Biol Chem 2003;278:35311–6.
12. Leuschner C, Enright FM, Gawronska B, Hansel W. Membrane disrupting lytic peptide conjugates destroy hormone dependent and independent breast cancer cells *in vitro* and *in vivo*. Breast Cancer Res Treat 2003; 78:17–27.
13. Papo N, Braunstein A, Eshhar Z, Shai Y. Suppression of human prostate tumor growth in mice by a cytolytic D-, L-amino acid peptide: membrane lysis, increased necrosis, and inhibition of prostate-specific antigen secretion. Cancer Res 2004;64:5779–86.
14. Ganz T, Lehrer RI. Defensins. Curr Opin Immunol 1994;6:584–9.
15. Epand RM, Vogel HJ. Diversity of antimicrobial peptides and their mechanisms of action. Biochim Biophys Acta 1999;15:1–2.
16. Shai Y. Mechanism of the binding, insertion and destabilization of phospholipid bilayer membranes by α-helical antimicrobial and cell non-selective membrane-lytic peptides. Biochim Biophys Acta 1999;1462: 55–70.
17. Tossi A, Sandri L, Giangaspero A. Amphipathic, α-helical antimicrobial peptides. Biopolymers 2000;55: 4–30.
18. Bulet P, Stocklin R, Menin L. Anti-microbial peptides: from invertebrates to vertebrates. Immunol Rev 2004; 198:169–84.
19. Shai Y. Mode of action of membrane active antimicrobial peptides. Biopolymers 2002;66:236–48.
20. Papo N, Shahar M, Eisenbach L, Shai Y. A novel lytic peptide composed of D, L amino acids selectively kills cancer cells in culture and in mice. J Biol Chem 2003; 278:21018–23.
21. Zwaal RF, Schroit AJ. Pathophysiologic implications of membrane phospholipid asymmetry in blood cells. Blood 1997;89:1121–32.
22. Zwaal RF, Comfurius P, Bevers EM. Surface exposure of phosphatidylserine in pathological cells. Cell Mol Life Sci 2005;62:971–88.
23. Chen HM, Wang W, Smith D, Chan SC. Effects of the anti-bacterial peptide cecropin B and its analogs, cecropins B-1 and B-2, on liposomes, bacteria, and cancer cells. Biochim Biophys Acta 1997;1336:171–9.
24. Chan SC, Yau WL, Wang W, Smith DK, Sheu FS, Chen HM. Microscopic observations of the different morphological changes caused by anti-bacterial peptides on *Klebsiella pneumoniae* and HL-60 leukemia cells. J Pept Sci 1998;4:413–25.
25. Papo N, Shai Y. New lytic peptides based on the D, L amphipathic helix motif preferentially kill tumor cells compared to normal cells. Biochemistry 2003;42:9346–54.
26. Manno S, Takakuwa Y, Mohandas N. Identification of a functional role for lipid asymmetry in biological membranes: phosphatidylserine-skeletal protein interactions modulate membrane stability. Proc Natl Acad Sci U S A 2002;99:1943–8.
27. Ellerby HM, Arap W, Ellerby LM, et al. Anti-cancer activity of targeted pro-apoptotic peptides. Nat Med 1999;5:1032–8.
28. Baker MA, Maloy WL, Zasloff M, Jacob LS. Anticancer efficacy of magainin 2 and analogue peptides. Cancer Res 1993;53:3052–7.
29. Patel BJ, Pantuck AJ, Zisman A, et al. CL1-GFP: an androgen independent metastatic tumor model for prostate cancer. J Urol 2000;164:1420–5.
30. Sramkoski RM, Pretlow TG II, Giaconia JM, et al. A new human prostate carcinoma cell line, 22Rv1. In Vitro Cell Dev Biol Anim 1999;35:403–9.
31. Okamoto M, Webber MM, Quader S, Oyasu R. Interleukin-6 and epidermal growth factor promote anchorage-independent growth of immortalized human prostatic epithelial cells treated with *N*-methyl-*N*-nitrosourea. Prostate 1998;35:255–62.
32. Gavish Z, Pinthus JH, Barak V, et al. Growth inhibition of prostate cancer xenografts by halofuginone. Prostate 2002;51:73–83.
33. Mabjeesh NJ, Escuin D, LaVallee TM, et al. 2ME2 inhibits tumor growth and angiogenesis by disrupting microtubules and dysregulating HIF. Cancer Cell 2003;3: 363–75.
34. Porgador A, Bannerji R, Watanabe Y, Feldman M, Gilboa E, Eisenbach L. Antimetastatic vaccination of tumor-bearing mice with two types of IFN-γ gene-inserted tumor cells. J Immunol 1993;150:1458–70.
35. Dadiani M, Margalit R, Sela N, Degani H. High-resolution magnetic resonance imaging of disparities in the transcapillary transfer rates in orthotopically inoculated invasive breast tumors. Cancer Res 2004;64: 3155–61.
36. Rosenfeld Y, Papo N, Shai Y. Endotoxin (lipopolysaccharide) neutralization by innate immunity host-defense peptides: peptide properties and plausible modes of action. J Biol Chem 2006;281:1636–43.
37. Matz MV, Fradkov AF, Labas YA, et al. Fluorescent proteins from nonbioluminescent Anthozoa species. Nat Biotechnol 1999;17:969–73.
38. Pouny Y, Shai Y. Interaction of D-amino acid incorporated analogues of pardaxin with membranes. Biochemistry 1992;31:9482–90.
39. Dings RP, Yokoyama Y, Ramakrishnan S, Griffioen AW, Mayo KH. The designed angiostatic peptide anginex synergistically improves chemotherapy and antiangiogenesis therapy with angiostatin. Cancer Res 2003;63: 382–5.
40. Van Blitterswijk WJ, De Veer G, Krol JH, Emmelot P. Comparative lipid analysis of purified plasma membranes and shed extracellular membrane vesicles from normal murine thymocytes and leukemic GRSL cells. Biochim Biophys Acta 1982;688:495–504.
41. Papo N, Oren Z, Pag U, Sahl HG, Shai Y. The consequence of sequence alteration of an amphipathic α-helical antimicrobial peptide and its diastereomers. J Biol Chem 2002;277:33913–21.
42. Papo N, Shai Y. Effect of drastic sequence alteration and D-amino acid incorporation on the membrane binding behavior of lytic peptides. Biochemistry 2004;43: 6393–403.
43. Liu CC, Walsh CM, Young JD. Perforin: structure and function. Immunol Today 1995;16:194–201.

Downloaded from http://aacrjournals.org/cancerres/article-pdf/66/10/5371/2548766/5371.pdf by guest on 16 January 2025